

Mass, total kinetic energy, and neutron multiplicity correlations in the binary fragmentation of $^{50}\text{Ti} + ^{208}\text{Pb}$ at 294 MeV bombarding energy

S. Appannababu,^{1,*} M. Cinausero,^{1,†} T. Marchi,^{1,‡} F. Gramegna,¹ G. Prete,¹ J. Bermudez,¹ D. Fabris,² G. Collazuol,^{2,3} A. Saxena,⁴ B. K. Nayak,⁴ S. Kailas,⁴ M. Bruno,⁵ L. Morelli,⁵ N. Gelli,⁶ S. Piantelli,⁶ G. Pasquali,^{6,7} S. Barlini,^{6,7} S. Valdré,^{6,7} E. Vardaci,⁸ L. Sajo-Bohus,⁹ M. Degerlier,¹⁰ A. Jhingan,¹¹ B. R. Behera,¹² and V. L. Kravchuk¹³

¹*I.N.F.N. Laboratori Nazionali di Legnaro, Italy*

²*I.N.F.N. Sezione di Padova, Italy*

³*Dipartimento di Fisica e Astronomia dell'Università di Padova, Italy*

⁴*Nuclear Physics Division, Bhabha Atomic Research Centre, Mumbai, India*

⁵*Sezione I.N.F.N. and Dipartimento di Fisica e Astronomia dell'Università di Bologna, Italy*

⁶*I.N.F.N. Sezione di Firenze, Italy*

⁷*Dipartimento di Fisica dell'Università di Firenze, Italy*

⁸*Sezione I.N.F.N. and Dipartimento di Scienze Fisiche, Università Federico II, Napoli, Italy*

⁹*Universidad Simon Bolivar, Caracas, Venezuela*

¹⁰*Nevsehir Haci Bektas University Science and Art Faculty Physics Department, Nevsehir, Turkey*

¹¹*Inter-University Accelerator Centre, New Delhi, India*

¹²*Department of Physics, Panjab University, Chandigarh, India*

¹³*National Research Centre "Kurchatov Institute," Moscow, Russia*

(Received 8 January 2016; revised manuscript received 17 August 2016; published 27 October 2016)

The correlations between mass distributions of the binary fragments, total kinetic energy (TKE), and neutron multiplicity have been investigated for the reaction $^{50}\text{Ti} + ^{208}\text{Pb}$ at 294 MeV bombarding energy. Although this reaction has been used to synthesize the Rf ($Z = 104$) superheavy element, a complete study of its fragmentation dynamics is still not available in the literature. In this work, average neutron multiplicities were extracted as a function of different fragment mass splits and TKE windows. A weak increase of the pre-scission neutron multiplicity is observed going from asymmetric to symmetric mass splits. A fission delay time of 4.5×10^{-20} s has been extracted for the symmetric fission. The neutron multiplicity extracted for the symmetric mass split was used to derive the average number of neutrons emitted in the spontaneous fission of ^{258}Rf . The extrapolated value of 4.7 ± 1.4 is found to be consistent with systematics of spontaneous and neutron-induced fission in heavy nuclei and with the results of previous works for superheavy nuclei with $Z = 116$ and $Z = 124$.

DOI: [10.1103/PhysRevC.94.044618](https://doi.org/10.1103/PhysRevC.94.044618)

I. INTRODUCTION

Several experimental efforts have been made to synthesize superheavy elements (SHEs) [1]. Such experiments are extremely challenging because the formation of SHEs is strongly hindered either by the equilibrium fission (or fusion-fission; FF) that proceeds through compound nucleus (CN) formation, or by nonequilibrium processes such as fast-fission, quasifission, and pre-equilibrium fission, generally grouped together as quasifission (QF).

The essential steps in the synthesis of SHEs are (i) the two heavy colliding nuclei overcome the Coulomb barrier to form a composite system, (ii) the composite system reaches the CN configuration, and (iii) the CN deexcites by neutron and gamma emission without undergoing fission. The CN survival probability with respect to fission depends on the height of the fission barrier, which is determined by nuclear shell corrections

in the superheavy region. Furthermore, the height of the barrier rapidly decreases with increasing excitation energy of the CN [2,3]. As a consequence, there is only a narrow bombarding energy window giving the optimum SHE-production cross section. In this context, two different classes of reactions are considered: “cold” and “hot” fusion. In cold fusion, spherical target nuclei such as Bi and Pb are used and the CN is formed at low excitation energy, so that only one neutron is emitted. In hot fusion, deformed actinide target nuclei are employed, the CN excitation energy is higher, and more than one neutron is emitted (generally from three to five).

In the case of massive interacting nuclei, the relative probability of QF processes with respect to CN formation depends on entrance channel parameters such as mass asymmetry, N/Z ratio, deformation, and orientation of the colliding nuclei shell structure [4–6]. As discussed by Swiatecki [7], the heavy-ion-induced fusion process depends on three milestone configurations of the colliding system: the touching configuration, the conditional saddle point at frozen mass asymmetry, and the unconditional saddle-point configuration. He also suggests reconsidering the dynamical factor of diffusion to account for the probability that the composite system reaches the compound nucleus configuration by thermal fluctuations, even when the system is formed below the Coulomb barrier.

*Present Address: Departamento de Fisica Nuclear - Instituto de Fisica - Universidade de Sao Paulo, Brazil.

†Corresponding author: cinausero@lnl.infn.it

‡Present Address: KU Leuven Department of Physics and Astronomical Instituut voor Kern- en Stralingsfysica, Leuven, Belgium.

All the above considerations point to the need to experimentally investigate the optimum conditions for CN formation. Since both the CN fission and QF correspond to full momentum transfer and can also result in similar mass distributions with significant yield in the symmetric mass splitting, the interpretation of the fusion-fission data is not straightforward, although correlation studies between different observables were performed. Fragment-mass–total-kinetic-energy correlations can be used to follow the evolution of the reaction mechanism from deep inelastic collisions (DICs) to QF and FF [8]. Furthermore, prescission neutron multiplicities can provide a clock for the fission timescale. In fact, QF and FF follow different paths in the evolution of the composite system, thus having different average timescales. The QF average times are expected to be shorter ($\leq 10^{-20}$ s) with respect to FF (typical values are in the range from $\sim 10^{-20}$ s up to 10^{-16} s). Determination of the total dynamical times from measured neutron multiplicities can thus give a signature of the reaction process.

In the past [9,10], fragment-fragment-neutron correlations have been studied for the binary fragmentation of the $^{56}\text{Fe} + ^{232}\text{Th}$, $^{80}\text{Se} + ^{208}\text{Pb}$, and $^{80}\text{Se} + ^{232}\text{Th}$ at center-of-mass energies from 300 to 470 MeV. The excitation energies of the equilibrated CN ($Z = 116$ and 124) range from 50 to 180 MeV. The average number of prompt spontaneous fission neutrons, ν_{sf} , of the superheavy nucleus for these systems was determined by extrapolating the neutron emission to zero excitation energy in the mass-symmetric split.

However, for these systems, no superheavy residues have been found. It is therefore of great interest to continue such studies for specific target-projectile combinations where the detection of evaporation residues (ERs) experimentally demonstrates that the CN-formation cross section is nonzero.

The $^{50}\text{Ti} + ^{208}\text{Pb}$ cold fusion reaction was used to synthesize the Rf element ($Z = 104$), but the study of its fragmentation dynamics [11,12] is still not complete. In a recent paper [13] the CN formation probability was estimated from the measurement of fission-fragment angular distributions up to a center-of-mass energy of 200 MeV. In the same paper the need of fragment-fragment-neutron correlation measurements was pointed out for this system. In this paper we report the results of the first fragment-fragment-neutron correlation experiment for the $^{50}\text{Ti} + ^{208}\text{Pb}$ reaction. The center-of-mass energy of 234 MeV was chosen to achieve a capture cross section high enough to perform the correlation measurement with reasonable statistics.

II. EXPERIMENTAL DETAILS

The experiment was performed at the TANDEM–ALPI accelerator facility of the Laboratori Nazionali di Legnaro (Italy). A 294 MeV ^{50}Ti beam of 0.5 pA intensity impinged on a stack of two self-supporting ^{208}Pb targets, each 500 $\mu\text{g}/\text{cm}^2$ thick. The binary fragments were detected with two time-of-flight (TOF) arms based on microchannel plates (MCPs) [14]. The two TOF arms were centered at $\theta_{\text{lab}} = \pm 65^\circ$ with an opening angle of $\pm 9.2^\circ$, to detect the complementary binary fragments as well as the elastically scattered events. Each TOF arm consists of a compact start detector and a position-sensitive

stop detector placed at a relative distance of 18 cm. The start detectors were positioned 6.8 cm from the target.

The start detector consists of a conversion foil, an accelerating grid, an electrostatic mirror, and a chevron MCP assembly. The stop detector consists of a conversion entrance foil, a chevron assembly of two MCPs, and a x - y coordinate system based on two mutually perpendicular delay lines. The x and y coordinates of the stop MCP were calibrated by using the edges of the stop detector active area and a reference grid placed in front of the entrance foil, to give the polar (θ) and azimuthal (ϕ) angles with respect to the beam axis. The calibration of the TOF spectrum of each arm was achieved by using the elastic-scattering events. A time resolution of about 300 ps (full width at half maximum; FWHM) and spatial resolution of about 500 μm (FWHM) were achieved in the present measurement.

Neutrons were detected by using 24 cylindrical ($5'' \times 5''$) liquid scintillators (RIPEN array [15]) placed around the scattering chamber 2 m from the target. Twenty-two of them were placed in the plane at the angles $\theta_{\text{lab}}^n = \pm 35^\circ, \pm 45^\circ, \pm 55^\circ, -65^\circ, \pm 75^\circ, -85^\circ, +95^\circ, \pm 105^\circ, \pm 115^\circ, \pm 125^\circ, \pm 135^\circ, -145^\circ, -155^\circ, -165^\circ$. Two of them were placed out of plane at the angles $\theta_{\text{lab}}^n = +53^\circ, \phi^n = 10^\circ$ and $\theta_{\text{lab}}^n = +53.7^\circ, \phi^n = -10^\circ$.

The neutron TOF was measured with respect to the MCP start detector signal. The absolute neutron TOF was determined by using the prompt- γ -ray peak as a reference. Neutron- γ discrimination was achieved by using the zero-crossing method [16]. Intrinsic neutron detection efficiency was calculated by Monte Carlo simulations as a function of the experimental neutron detection threshold [9,10,15]. The energy detection threshold was determined by calibrating the energy deposited in the scintillators with ^{60}Co , ^{137}Cs , and ^{54}Mn γ sources.

A custom digital data-acquisition system was used. The hardware was based on CAEN digitizing boards, properly selected according to the signal properties of each detector. The 1 GS/s (10 bit, 1 Vpp) V1751 module was employed for digitizing the fast start and stop MCP signals, while for the liquid scintillators the 250 MS/s (12 bit, 2 Vpp) V1720 board was chosen. The latter module has also been used to acquire the x and y MCP signals (after analog integration through a timing filter amplifier). The sampled waveforms have been registered event by event and processed off-line to extract energy and timing information, as well as MCP's x and y coordinates and the scintillator's pulse shape factor (zero crossing) for neutron- γ discrimination. A custom trigger-box module was also developed by using the CAEN V1495 FPGA board [17]. This allowed us to synchronize the data acquisition among the different boards and to provide a versatile trigger selection.

The trigger for data acquisition was generated from double and triple coincidences between start and stop of each MCP and at least one neutron detector.

III. DATA ANALYSIS AND RESULTS

The goal of the data analysis was to reconstruct the total kinetic energy (TKE) and the mass distribution of the binary

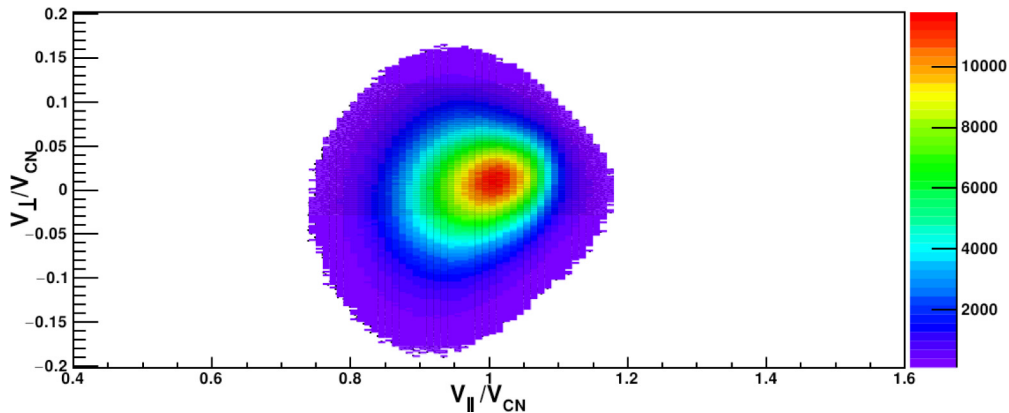


FIG. 1. Two-dimensional plot of V_{\parallel}/V_{CN} vs V_{\perp}/V_{CN} distribution for the $^{50}\text{Ti} + ^{208}\text{Pb}$ reaction at 294 MeV bombarding energy.

fragments and to correlate them with the number of emitted neutrons.

The velocity vectors of the detected fragments were built by using the measured TOF and emission polar and azimuthal angles (θ and ϕ). Proper corrections were applied to account for the energy lost by the fragments in the target and in the entrance window of the start MCP. A proper “time zero” correction was also applied to take into account the flight time of each fragment traveling from the target to the entrance window of the reference start MCP. This correction is needed in order to extract the actual TOF of the emitted neutrons and to determine their energies. From the measured velocities, provisional fragment masses and kinetic energies were calculated by assuming binary kinematics, linear momentum, and mass-conservation relationships. Final values were then obtained by starting from the provisional ones in an iterative procedure until convergence, as discussed in Refs. [14,18]. The measure of the azimuthal angles of the fragments ϕ provides a check of the coplanarity of the emission that is a characteristic of the binary (two-body) events. In the present case the azimuthal folding angle of the measured coincident fragments is $\phi_{12} = 180^\circ$, (FWHM) = 6° , thus demonstrating the coplanarity of the two emitted fragments. The recoil velocity components of the composite system, parallel (V_{\parallel}) and perpendicular (V_{\perp}) to the beam axis, were determined event by event from the measured folding angle and velocities of the two coincident fragments, following the procedure given in Ref. [19]:

$$V_{\parallel} = \frac{u_1 w_2 + u_2 w_1}{u_1 + u_2}, \quad (1)$$

and

$$V_{\perp} = \frac{u_1 u_2 \sin \phi_{12}}{\sqrt{u_1^2 + u_2^2 - 2u_1 u_2 \cos \phi_{12}}}, \quad (2)$$

where $u_i = v_i \sin \theta_i$, $w_i = v_i \cos \theta_i$, and v_i and θ_i are, respectively, the velocities and the polar angles measured in the laboratory reference frame for the two fragments ($i = 1, 2$). ϕ_{12} is the azimuthal folding angle as already defined above.

Binary-fragmentation events with full momentum transfer are characterized by $V_{\parallel}/V_{CN} = 1$ and $V_{\perp} = 0$. The reconstructed V_{\parallel}/V_{CN} and V_{\perp}/V_{CN} are shown in the two-

dimensional intensity plot of Fig. 1. The reconstructed values are $V_{\parallel}/V_{CN} = 0.98$ (FWHM) = 0.19, $V_{\perp}/V_{CN} = 0.0$ (FWHM) = 0.1, which demonstrate the full momentum transfer of the binary events.

A. Total kinetic energy and fragment mass correlations

The upper panel of Fig. 2 presents the experimental two-dimensional plot of the center-of-mass total kinetic energy (TKE) versus the mass of the coincident fragments. Mass and energy resolutions of ~ 4.5 mass units and ~ 10 MeV (FWHM), respectively, have been obtained in the present measurement. The fragment-mass–TKE plot is dominated by events close to the target and projectile masses which correspond to elastic, quasi-elastic, and deep-inelastic collisions. The FF and QF events are located in the intermediate region between $A \simeq 70$ and $A \simeq 190$. Fusion-fission is supposed to mainly take place in the symmetric splitting region $A = 129 \pm 20$. In Fig. 2 (lower panel) the experimental average TKE ($\langle \text{TKE} \rangle$) is also reported as a function of fragment mass in the $70 < A < 180$ region. The reported experimental $\langle \text{TKE} \rangle$ values were corrected for prompt neutron evaporation according to the recipe given in Ref. [21]. The predicted value from the Viola systematics [20] is shown as a dashed line. The line has a parabolic dependence on the fragment mass as predicted by the liquid drop model and it is independent of the CN excitation energy [22]. In the same figure, the $\langle \text{TKE} \rangle$ values predicted by the Itkis systematics [23] are also shown as a solid line. The experimental $\langle \text{TKE} \rangle$ values are between the two systematics, indicating a fair agreement with the liquid drop model of fission.

The $\langle \text{TKE} \rangle$ values reconstructed from fragment-fragment events in coincidence with neutrons do not show significant differences with respect to what is reported above. The FWHM of the TKE distribution in the considered mass region ($70 < A < 180$) is about 70 MeV. If we apply cuts of 10 u in the mass interval considered above, the FWHM of the TKE distribution grows from about 45 to 70 MeV, going from the very asymmetric to the symmetric mass split. Those values are compatible with the ~ 50 MeV value predicted by Itkis [23] and the experimental value of 45 MeV reported in Ref. [11]. The mass-yield distribution for different TKE selection is reported in Fig. 3.

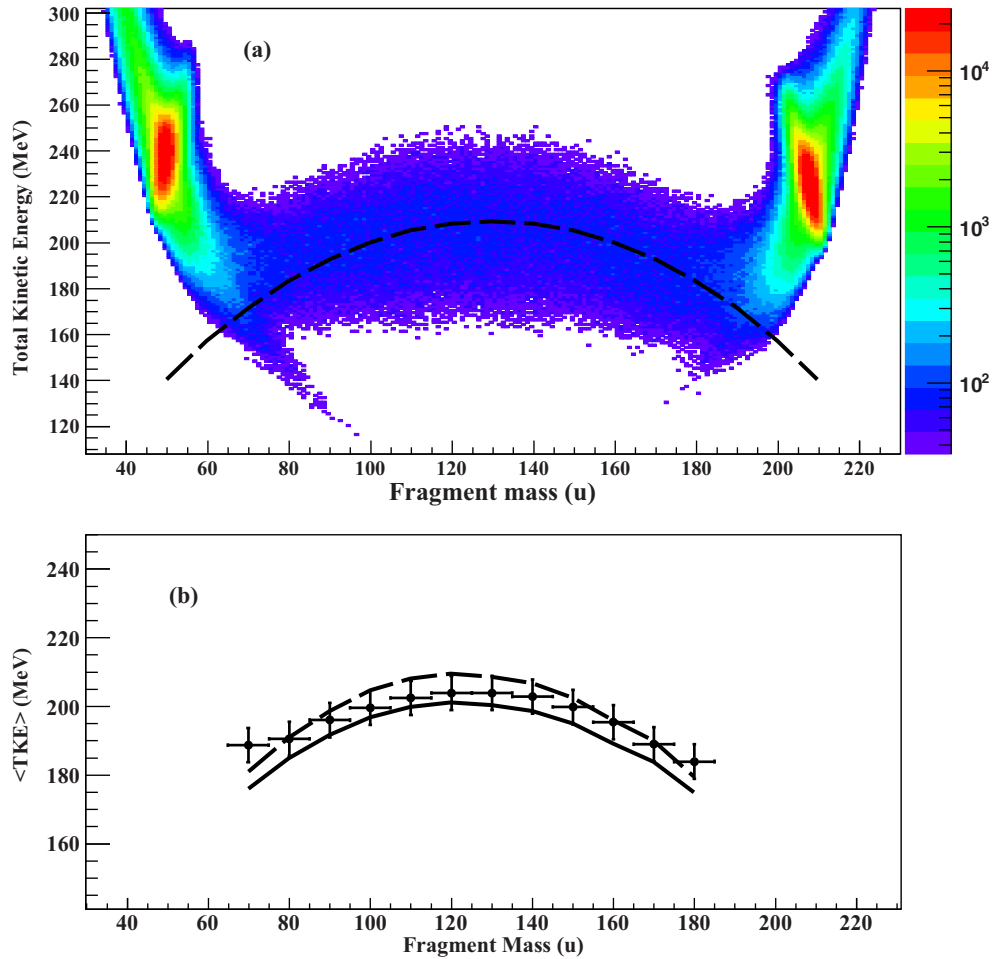


FIG. 2. (a) Scatter plot of total kinetic energy vs fragment mass. The dashed line is the average TKE ($\langle TKE \rangle$) from the Viola systematics [20]. (b) Variation of the measured $\langle TKE \rangle$ with the fragment mass compared with the predicted values from Viola (dashed line) and Itkis systematics (solid line). The horizontal error bars indicate the width of the fragment mass cuts, while the vertical error bars indicate the uncertainty of the TKE centroid.

The total distribution shown in Fig. 3(a) displays two relatively narrow peaks centered at the projectile and target masses and are relative to elastic, quasi-elastic, and deep inelastic reaction channels. The wide bump centered at the symmetric split ($A = 129$) is related to fission-like fragments. This bump is compared with the Gaussian distribution predicted by the systematics for symmetric mass splitting [23]. This systematics relies on a large set of experimental data, including the work of Bock *et al.* [11] and predicts for the present case a FWHM of about 60 mass units. As shown in the figure this value is significantly lower with respect to the FWHM of the measured distribution. This comparison seems to indicate for the present system a non-negligible contribution from asymmetric fission.

We stress the fact that the Itkis systematics [23] does not take into account asymmetric splitting. Quasi-elastic and deep-inelastic collisions do not give any contribution to the symmetric mass region because only few nucleons are exchanged between target and projectile nuclei.

As reported in Figs. 3(b) and 3(c), the symmetric fragmentation contribution (mainly related to fusion-fission) increases

with increasing TKE. This is consistent with the fact that higher TKE means that the composite system has reached more compact shapes.

B. Neutron emission

Because in general FF and QF events may result in similar mass distributions, the contribution of fusion-fission can be better identified through neutron multiplicities in correlation with binary fragments. For this purpose, we analyzed the measured neutron spectra by dividing the mass-TKE distribution into three different mass splits: symmetric ($A = A_{CN}/2 \pm 20$), asymmetric ($70 < A < 110$) and projectile-like fragments (PLFs) ($40 < A < 70$). The width of the mass cuts was chosen in order to have a reasonable statistics in the 24 coincident neutron spectra obtained for each cut to perform the multiple-source least-squares fitting procedure described below to extract pre- and postscission neutron multiplicities. Each neutron spectrum was assumed to be produced by the convolution of three moving sources: the compound nucleus formed after a complete fusion reaction and two

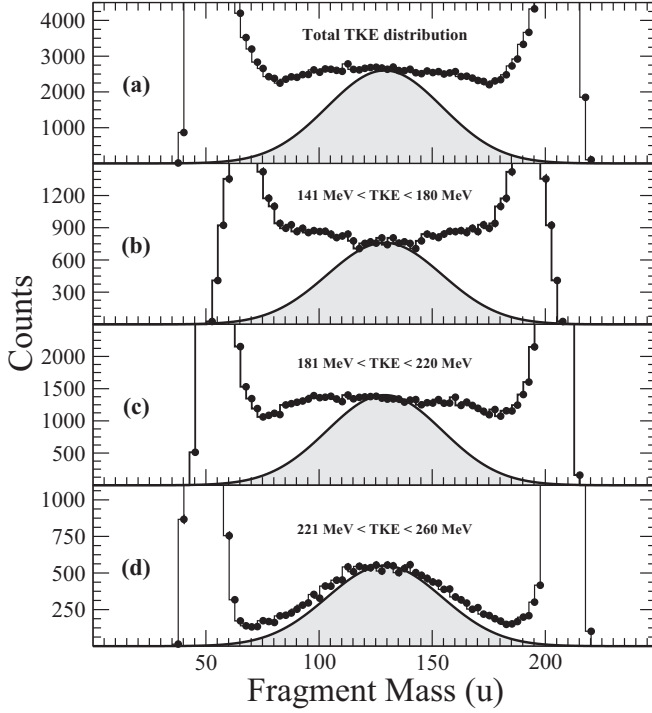


FIG. 3. Mass-yield distribution for 294 MeV $^{50}\text{Ti} + ^{208}\text{Pb}$ reaction: (a) total distribution, (b)–(d) mass yield for three different cuts in the TKE distribution. The average TKE increases from (b) to (c). The gray area indicates the Gaussian-like mass distribution from symmetric fission systematics. This distribution is normalized to the data at symmetric splitting for comparison. For details see the text.

correlated fission fragments after full acceleration. Neutrons were assumed to be emitted isotropically in the center-of-mass frame of each source following a Maxwellian distribution [24]. The transformation in the laboratory reference frame gives the Watt expression [25] summed over the three sources that reads

$$\frac{d^2 v_n^{\text{tot}}}{dE_n d\Omega_n} = \sum_{i=1}^3 \frac{v_n^i \sqrt{E_n}}{2(\pi T^i)^{3/2}} \exp \left[-\frac{E_n - 2\sqrt{E_n} \epsilon^i \cos \Psi^i + \epsilon^i}{T^i} \right], \quad (3)$$

where E_n is the measured neutron energy in the laboratory frame, ϵ^i and T^i are the energy per nucleon and temperature of the CN and the fission fragments F_1 and F_2 , v_n^i is the multiplicity of the neutron emitted by each source (CN, F_1 , and F_2). Ψ^i is the relative angle between the emitting source (CN, F_1 , and F_2) and the neutron detection angle. The value of ϵ^i for the CN was calculated assuming full momentum transfer. The ϵ^i values for the two fission fragments were taken from the Viola systematics [20]. In the case of the PLF mass cut, ϵ^i is taken from classical kinematical calculations. We stress the fact that these values are not so far from the reconstructed ones, as discussed in the previous section. The considered fragment-folding angles are the measured angles for each mass cut and are in agreement with Viola systematics and kinematical calculations.

The 24 neutron spectra for each mass cut were simultaneously fit with Eq. (3) in a least-squares fitting procedure. T^i

and v_n^i are the free parameters of the fits. The iterative fitting procedure ends when a convergence with same parameters is achieved for all spectra at all angles. The angular acceptance of both neutron and fission-fragment detectors is taken into account while calculating the relative angle Ψ^i between the direction of the emitted neutron and its source. Neutron pre- and postscission components can be separated because of their different angular correlations. In fact, the postscission neutrons are correlated with the fragment directions while precission neutrons are correlated with the direction of the thermalized CN.

The total average neutron multiplicity is thus obtained as $\nu_{\text{tot}} = \nu^{\text{CN}} + \nu^{F1} + \nu^{F2}$, where ν^{CN} is the average neutron multiplicity from the composite system, i.e., the precission component ν_{pre} , ν^{F1} and ν^{F2} are the average neutron multiplicities from the two binary fragments giving the postscission component as $\nu_{\text{post}} = \nu^{F1} + \nu^{F2}$.

Typical fits of the neutron multiplicity spectra are shown in Fig. 4 for the symmetric mass split. In the figure are reported the relative angles of the detected neutron with respect to the fragments (F1 and F2) and the contribution to the total spectra of the precission neutrons and of postscission neutrons coming from fragments F1 and F2.

The values of ν_{pre} , ν_{post} , and ν_{tot} for the different mass cuts are shown in Table I.

In the PLF mass cut, as expected, a very low total neutron multiplicity is obtained ($\nu_{\text{tot}} = 0.42 \pm 0.03$). A weak dependence with the mass asymmetry of both ν_{tot} and ν_{pre} is observed in going from the asymmetric to the symmetric split even if the multiplicity values are compatible within the error bars. We stress the fact that the best-fit values of ν_{pre} and ν_{post} reported in Table I for these two mass cuts are in fair agreement with the values $\nu_{\text{pre}} = 1.9$ and $\nu_{\text{post}} = 6.4$ predicted by the Itkis systematics [23]. Best-fit temperatures of $T_{\text{pre}} = 2.4 \pm 0.8$ MeV and $T_{\text{post}}^{F1} = T_{\text{post}}^{F2} = 1.9 \pm 0.1$ MeV ($T_{\text{pre}} = 1.8 \pm 0.8$ MeV, $T_{\text{post}}^{F1} = 1.6 \pm 0.1$ MeV, $T_{\text{post}}^{F2} = 1.5 \pm 0.1$ MeV) are derived for the symmetric (asymmetric) mass cut. The corresponding minimum reduced χ^2 values are about 1.4 in both cases. The errors take into account a reduced χ^2 variation of 10% and includes correlations of ν_{pre} and ν_{post} with T_{pre} and T_{post} .

The energy balance of the reaction process for the different mass cuts can be derived by using the experimental neutron multiplicity along with the measured total kinetic energy [9,10].

The available excitation energy for a particular channel can be written as

$$E_{\text{avail}} = E_{\text{c.m.}} + Q_{\text{gg}} - \langle \text{TKE} \rangle = E_{\text{CN}}^x + Q_{\text{Fiss}} - \langle \text{TKE} \rangle, \quad (4)$$

where $E_{\text{c.m.}}$ is the available energy in the center of mass (i.e., 234 MeV in the present case), E_{CN}^x the excitation energy of the compound nucleus (i.e., 64 MeV for the present reaction), Q_{gg} is the Q value for the selected exit channel with respect to the entrance channel (projectile-target combination), Q_{Fiss} is the Q value for the CN fission, and $\langle \text{TKE} \rangle$ is the total kinetic energy of the binary fragments. In the case of symmetric (asymmetric) split $Q_{\text{gg}} = 101$ MeV (66 MeV),

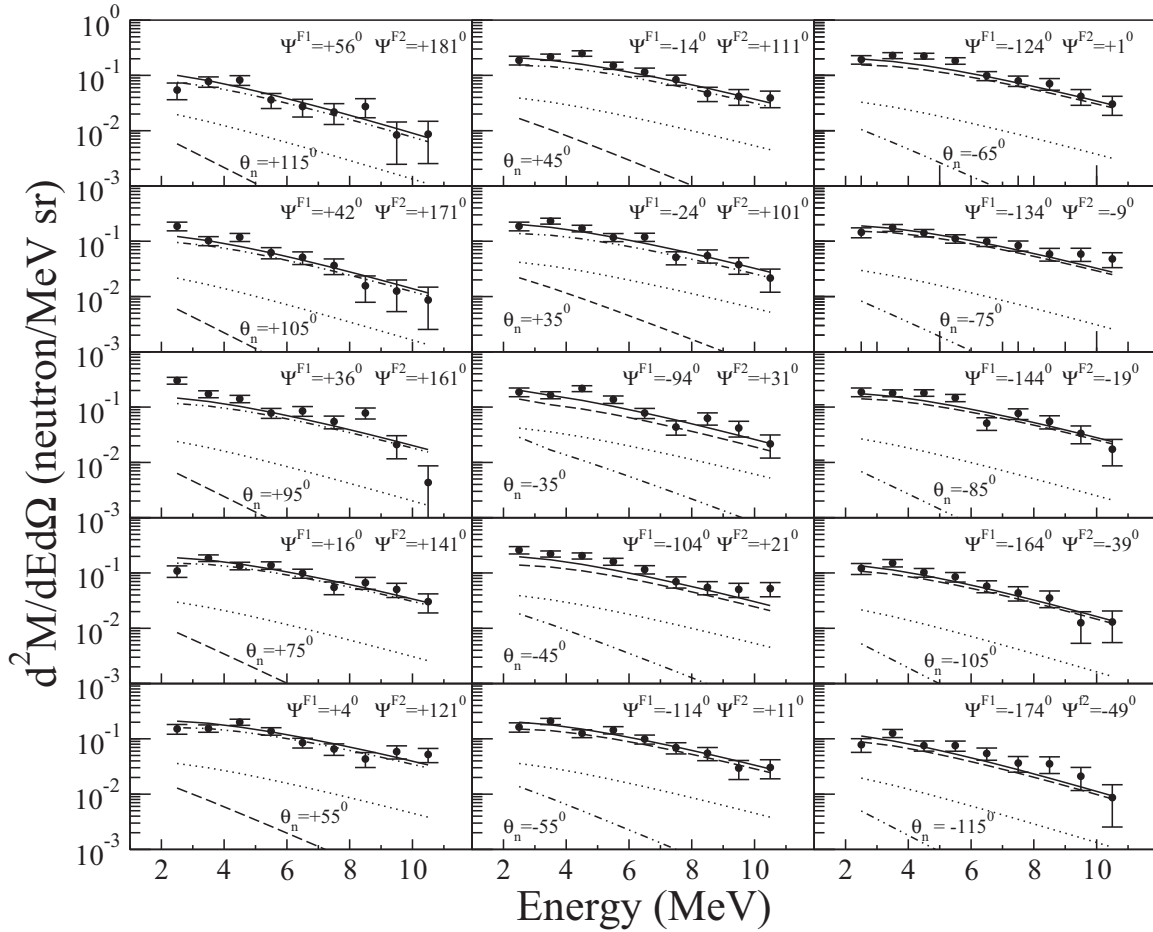


FIG. 4. Experimental (full circles) double differential neutron energy spectra at different angles with respect to the beam direction for the symmetric mass split ($A = A_{CN}/2 \pm 20$). Multisource fits to the data are also shown: solid curves correspond to the total neutron emission, dotted curves correspond to the pre-scission neutron emission, dot-dashed curves to post-scission neutron from fragment F1 and dashed curves from fragment F2. The relative angles between the detected neutron and the two fragments are also indicated.

$Q_{\text{Fiss}} = 270$ MeV (236 MeV) and $\langle \text{TKE} \rangle = 204 \pm 5$ MeV (196 ± 5 MeV) leading to $E_{\text{avail}} = 131 \pm 10$ MeV (104 ± 10 MeV). Consequently, the average overall energy cost for the emission of a single neutron (ΔE_n) = $E_{\text{avail}}/\nu_{\text{tot}}$ is 14 ± 3 MeV (13 ± 3 MeV) for symmetric (asymmetric) split. This overall neutron cost also includes the emission of γ rays along the deexcitation cascade. The ΔE_n value found in the present experiment is in nice agreement with the 14 MeV value found for the fission of the ^{260}Rf nucleus formed in the reaction $^{28}\text{Si} + ^{232}\text{Th}$ at 340 MeV bombarding energy [26]. From the estimated average energy cost for neutron emission one can also estimate the neutron multiplicity for the spontaneous fission of the ^{258}Rf as $\nu_{\text{sf}} = Q_{\text{eff}}/\Delta E_n = 4.7 \pm 1.4$. Q_{eff} is the

effective Q value for fission defined as $Q_{\text{eff}} = Q_{\text{Fiss}} - \langle \text{TKE} \rangle$ and represents the available energy for fission when the CN is populated in its ground state. The value $\nu_{\text{sf}} = 4.7 \pm 1.4$ is consistent with systematics of spontaneous and neutron-induced fission on heavy nuclei [25,26] and with the findings of previous works [9,10] for the superheavy nuclei $Z = 116$ and $Z = 124$.

The ν_{tot} value extracted in the symmetric mass split can be compared with published data [10,27,28] on composite systems with $Z \geq 100$ in an excitation-energy window of $64 \text{ MeV} \leq E^x \leq 74$ MeV. This comparison is reported in Fig. 5 (upper panel) and shows that, at the same compound nucleus excitation energy, there is a smooth increase of the

TABLE I. Neutron multiplicities for the reaction $^{208}\text{Pb}(^{50}\text{Ti}, f)$ as a function of different mass cuts.

Neutron multiplicities	PLF mass cut $40 < A < 70$	Asymmetric mass cut $70 < A < 110$	Symmetric mass cut $109 < A < 149$
ν_{pre}	0.15 ± 0.02	1.9 ± 0.8	2.2 ± 0.8
ν_{post}	0.27 ± 0.02	6.3 ± 0.6	6.8 ± 0.4
ν_{tot}	0.42 ± 0.03	8.2 ± 1.0	9.0 ± 0.9

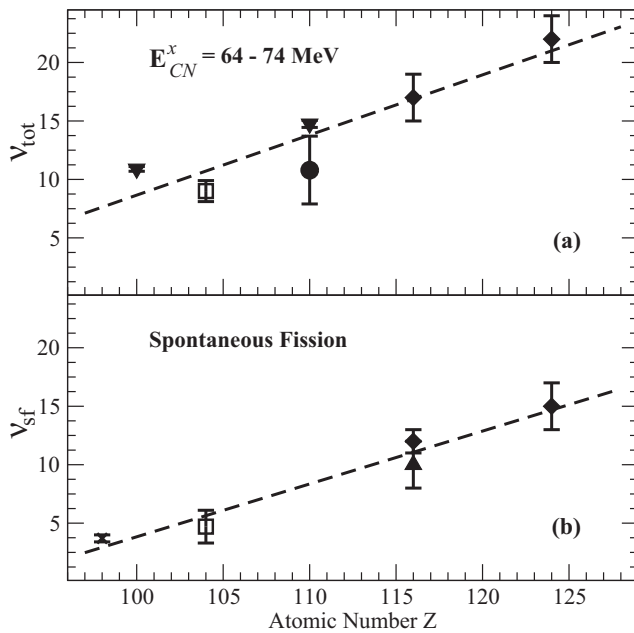


FIG. 5. (a) Variation of ν_{tot} with atomic number of composite nucleus in the excitation-energy range 64–74 MeV. Full diamonds are from Ref. [10], full down triangles from Ref. [27], and full circles from Ref. [28]. Open squares show the result of the present experiment. (b) Variation of ν_{sf} with atomic number of composite nucleus. Full diamonds are from Ref. [10], full up triangles from Ref. [9], the cross represents the ^{252}Cf spontaneous fission datum. Open squares show the result of the present experiment.

total neutron multiplicity of about 0.5 neutrons per unit atomic number Z . The slope of this variation is similar to the value reported in Ref. [10] for different excitation-energy windows. A comparable smooth increase of 0.45 neutrons per unit atomic number is also found when comparing the present ν_{sf} value with spontaneous fission neutron multiplicity for $Z = 116$, $Z = 124$ [9,10], and ^{252}Cf ($Z = 98$) nuclei, as shown in the lower panel of Fig. 5.

To further investigate the reaction dynamics, the TKE dependence of the neutron multiplicities were studied, performing the multiple source fitting procedure for different TKE gates. However, straight cuts in TKE will give different mass yields for each TKE window, as discussed in the previous section and shown in Fig. 3. Thus, following the procedure described in Ref. [27], these gates have been built considering linear cuts in the ratio, RTKE, between the measured TKE and the calculated TKE from Viola systematics [20] for a given mass asymmetry $R_F = A_{F1}/A_{F2}$ of the two emitted fragments. The appearance of such gates on the TKE-fragment mass plane is shown in the upper panel of Fig. 6. The width and the number of the RTKE gates have been chosen in order to reach a reasonable statistics to perform the multisource fitting procedure for each gate.

In the lower panel of Fig. 6, the total projection of the TKE in the selected fragment mass range ($85 < A < 175$) is shown together with the deduced pre-scission, post-scission, and total neutron multiplicities for the three considered cuts on RTKE. The deduced neutron multiplicities are plotted at

the mean TKE corresponding to each of the gates shown in the upper panel. The pre-scission multiplicity is found to increase steeply with increasing TKE. As discussed in Refs. [27,29,30], ν_{pre} should be almost independent from TKE in the case of fusion-fission. An increase of ν_{pre} with increasing TKE was also reported in the case of a reaction induced by $^{16,18}\text{O}$ and $^{36,40}\text{Ar}$ projectiles [27,29] and was explained with the recoil effect related to the evaporated particles [27,31].

Finally, we would like to stress the fact that a clear signature of the quasifission process should be, indeed, the reverse trend, i.e., the decrease of ν_{pre} with increasing TKE, as discussed in detail in Refs. [27,30]. In fact, in the case of quasifission, the neutron lifetime can be significantly shorter than the acceleration time of the fragments so that the hypothesis made for the fitting procedure that the neutrons are emitted from fully accelerated fragments is no longer valid. Consequently, neutrons emitted after scission but before the fragments have reached their asymptotic velocities are identified as pre-scission neutrons in the fits. The number of this “spurious” pre-scission neutrons sensitively depends on TKE, since high TKE means low excitation energy and thus fewer acceleration neutrons, while low TKE correspond to high excitation energy.

IV. DISCUSSION

A. Statistical model calculations

Statistical model calculations that include a fission delay are commonly used to get an estimate of the total fission timescales due to dynamical effects arising from nuclear viscosity. The simplest approach assumes that fission is totally hindered in the decay of the compound system up to a delay time τ_D . Consequently, for time $\tau < \tau_D$ the compound nucleus deexcites only by particle emission. This delay time τ_D used in the statistical model calculations represents the average time that the system needs to reach the scission point. In this way the experimental pre-scission multiplicities can be reproduced empirically by adjusting the fission delay time τ_D , treated as a free parameter. In the present case we used the PACE2 [32] statistical model code. As in the case of previous works on the SHE region [9,26] a level density parameter $a = A/10 \text{ MeV}^{-1}$ and a ratio $a_v/a_f = 1.0$ (a_v and a_f are the level density parameters for the residual nucleus and at the saddle point, respectively) have been chosen for the calculations. It is found that a fission delay of $4.5 \times 10^{-20} \text{ s}$ is required to account for the extracted pre-scission neutron multiplicity for the symmetric mass split and a fission delay of $2.8 \times 10^{-20} \text{ s}$ for the asymmetrical one. Taking into account the errors on the extracted ν_{pre} (see Table I), PACE2 calculations give a lower limit for the fission time of about $2.4 \times 10^{-20} \text{ s}$ ($2.3 \times 10^{-20} \text{ s}$) for the symmetric (asymmetric) mass cut. An upper limit of $1.3 \times 10^{-18} \text{ s}$ ($6.3 \times 10^{-20} \text{ s}$) for the symmetric (asymmetric) mass split was deduced by these calculations. The high upper limit set by the PACE2 statistical model for the symmetric mass window gate is due to the fact that, for the present case of ^{258}Rf at $E_{CN}^x = 64 \text{ MeV}$, the calculated number of pre-scission neutrons increases steeply up to $\tau_D = 10^{-19} \text{ s}$; beyond this value the ν_{pre} variation with the fission delay time becomes almost flat.

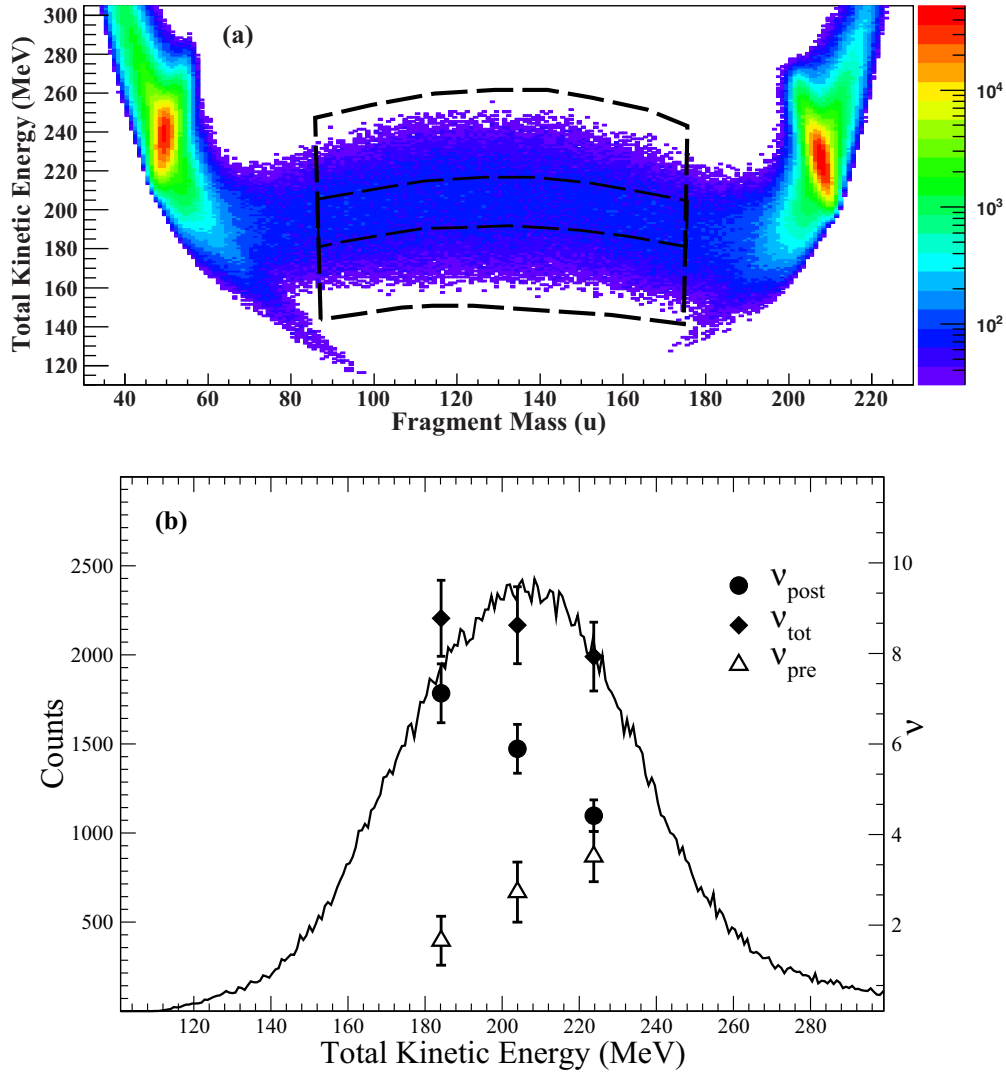


FIG. 6. (a) The three cut applied in the TKE vs fragment mass plane for the study of the TKE dependence of the neutron multiplicity. (b) Total projection of TKE in the selected mass range together with the deduced pre-scission (open triangles), single fragment post-scission (full circles), and total (full diamonds) neutron multiplicities plotted at the mean TKE of the gates in the fragment mass vs TKE plane shown in the upper panel.

The fission delay values found in the present case compare well with the value $\tau_D = 5_{-3}^{+7} \times 10^{-20}$ s reported in Ref. [26] for the decay of the ^{260}Rf at the excitation energy of about 180 MeV.

The extracted τ_D value for the symmetric split is longer with respect to the asymmetric split. This result is in agreement with the work of Hinde *et al.* [27] where the reduction of ν_{pre} for the asymmetric mass split in fusion-fission reactions was explained with a combination of phase-space effects and a reduction of the fission timescale for the more asymmetric mass splits.

B. Dynamical calculations

Dynamical calculations were also performed to get more insight into the experimental results. In particular, we calculate the dynamical trajectories with the HICOL code based on the original work of Feldmeier [33]. In this code, the evolution

of the two colliding nuclei for different values of the orbital angular momentum L is described by a sequence of shapes consisting of two spheres connected by a conical neck. The shapes are fully characterized by three macroscopic variables: the elongation s , i.e., the distance between the colliding nuclei (two sphere centers), the neck coordinate σ , and the entrance channel mass asymmetry Δ . The last two coordinates are defined as

$$\sigma = \frac{1}{V_0} \left(V_0 - \frac{4\pi}{3} R_1^3 - \frac{4\pi}{3} R_2^3 \right), \quad (5)$$

$$\Delta = \frac{R_1 - R_2}{R_1 + R_2}, \quad (6)$$

where V_0 is the total volume of the system that is assumed to be constant, R_1 and R_2 are the radii of the two interacting nuclei. The calculations assume a one-body dissipation function and the evolution is followed by solving the Langevin equations

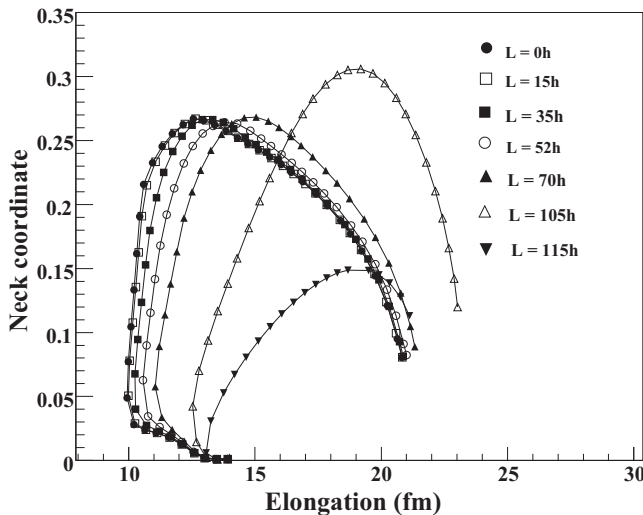


FIG. 7. Neck coordinate σ versus elongation s for dynamical trajectories calculated with the HICOL code at different values of the orbital angular momentum L for the $^{50}\text{Ti} + ^{208}\text{Pb}$ system at 294 MeV bombarding energy.

of motion. In Fig. 7 the calculated trajectories in the (s, σ) plane for the $^{50}\text{Ti} + ^{208}\text{Pb}$ system at 294 MeV bombarding energy are shown for different orbital angular momenta. These trajectories are typical nonfusion events. In fact, also at zero angular momentum, when the two colliding nuclei approach each other, the composite system develops a large neck and then re-separates into two fragments without reaching the fusion condition. On the contrary, for a fusion event the calculated trajectory ends when the minimum elongation is reached (see, e.g., Ref. [26]). The mass asymmetry of the two final fragments increases as a function of the angular momentum and at the highest L ($110\hbar$ – $130\hbar$) the system does not fully equilibrate in the mass degree of freedom and re-separates as projectile- and target-like fragments.

As a conclusion, HICOL calculations only predict QF events for the $^{50}\text{Ti} + ^{208}\text{Pb}$ system at the considered bombarding

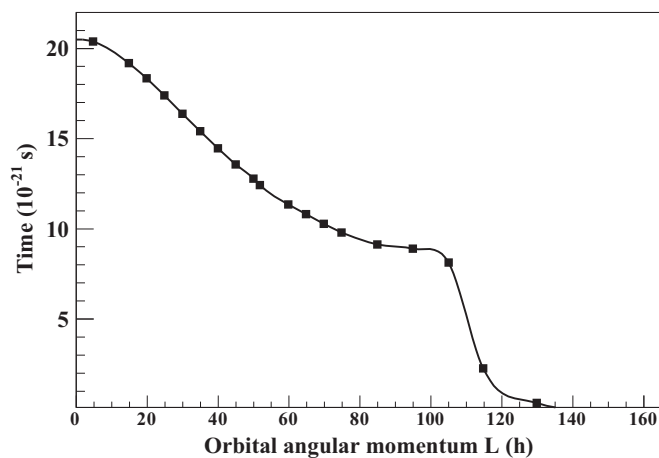


FIG. 8. Fission time as a function of the orbital angular momentum calculated with the HICOL code [33] for the $^{50}\text{Ti} + ^{208}\text{Pb}$ system at 294 MeV bombarding energy.

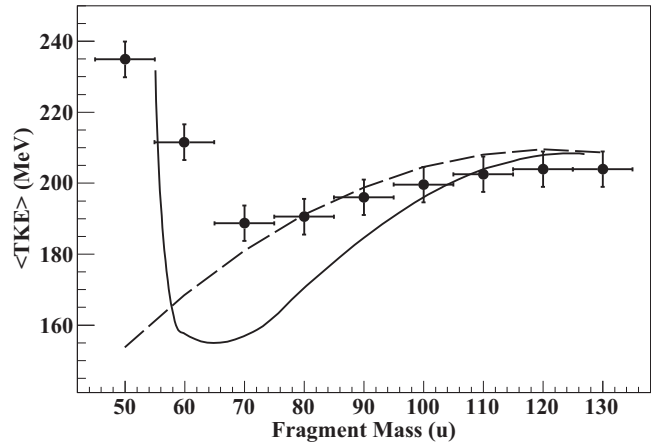


FIG. 9. Variation of the average TKE as a function of fragment mass along with the predictions of HICOL [33] (solid line) and Viola systematics [20] (dashed line).

energy. The contact to scission times as a function of the angular momentum can be also extracted from the evolution of the trajectories and are shown in Fig. 8. These times range from 2×10^{-20} s at $L = 0\hbar$ down to 8×10^{-21} s at $L = 100\hbar$, giving an average time of about 1×10^{-20} s. Because the HICOL code predicts only QF events for the system under study, these values are smaller with respect to the PACE2 results.

In Fig. 9 the variation of the average TKE as a function of the final fragment mass predicted by the HICOL code is shown as a solid curve. In the same figure this variation is compared with the Viola systematics (dashed line) and with the experimental values (full circles). The HICOL and Viola curves are very similar for the near-symmetric mass splittings and both in agreement with experimental values of $\langle \text{TKE} \rangle$. For the asymmetric mass splits, the experimental $\langle \text{TKE} \rangle$ is in better agreement with the Viola systematics. HICOL calculations are in substantial agreement with the experimental values for the quasi-elastic channels. From this comparison a possible small contribution of QF in the mass symmetric division cannot be completely ruled out for the system under study.

V. SUMMARY AND CONCLUSIONS

Fragment-mass–TKE distributions along with neutron multiplicities were measured in the binary fragmentation of the system $^{50}\text{Ti} + ^{208}\text{Pb}$ at 294 MeV bombarding energy. The results of the present study are consistent with a fusion-fission process with possible small contribution coming from quasi-fission events. This is supported by the observed fragment mass and TKE dependence of the pre-scission neutron multiplicity. Moreover, the values of $\langle \text{TKE} \rangle$ as a function of fragment mass are consistent with Viola [20] and Itkis [23] systematics characterizing the fusion-fission process. On the other hand, in the symmetric mass split, the experimental $\langle \text{TKE} \rangle$ values compare equally well with both Viola systematics and HICOL dynamical calculations, so that a possible admixture of quasi-fission events cannot be completely ruled out from the present analysis. PACE2 statistical model calculations including a fission delay time τ_D were used to deduce fission timescales

from the experimental precession neutron multiplicity. The extracted fission time is somewhat shorter for asymmetric than for symmetric mass splits, in agreement with earlier studies [27]. In particular, for the near symmetric events ($A_{CN}/2 \pm 20$) we found $\nu_{pre} = 2.2 \pm 0.8$, which corresponds to a fission delay of 4.5×10^{-20} s that compares well with the results of a previous work on the $^{28}\text{Si} + ^{232}\text{Th}$ system [26]. The total neutron multiplicity extracted in the case of symmetric mass division was used to derive the average neutron multiplicity for the spontaneous fission of the superheavy nucleus ^{258}Rf . The estimated value of $\nu_{sf} = 4.7 \pm 1.4$ was found to be consistent with previous results for $Z = 116$ and $Z = 124$ superheavy elements [9,10] and with systematics of spontaneous and neutron-induced fission of heavy nuclei [25,26].

The present work describes for the first time a fragment-fragment-neutron correlation measurement for the $^{50}\text{Ti} + ^{208}\text{Pb}$ system. Further studies with improved statistics

are needed to follow the evolution of the binary fragmentation of the system with the bombarding energy and to obtain a quantitative estimate of the fusion-fission and quasi-fission contributions to the reaction cross section.

ACKNOWLEDGMENTS

We wish to thank the staff of the Laboratori Nazionali di Legnaro for providing excellent beam quality and for the smooth operation of the TANDEM ALPI accelerator. We warmly thank V. Paticchio, G. Fiore, E. Fiore, and G. d'Erasmus (INFN Bari), and A. Olmi (INFN Firenze) and S. S. Kapoor (BARC Mumbai) for fruitful discussions. This work has been performed under the INFN-BARC collaboration and partially funded by INFN (Commissione III, esperimento NUCL-EX) and by the Italian "Ministero dell'Istruzione, dell'Università e della Ricerca" (Project 2010TPSCSP).

-
- [1] J. H. Hamilton, S. Hofmann, and Y. T. Oganessian, *Annu. Rev. Nucl. Part. Sci.* **63**, 383 (2013).
- [2] J. A. Sheikh, W. Nazarewicz, and J. C. Pei, *Phys. Rev. C* **80**, 011302(R) (2009).
- [3] J. C. Pei, W. Nazarewicz, J. A. Sheikh, and A. K. Kerman, *Phys. Rev. Lett.* **102**, 192501 (2009).
- [4] I. Dragojević, K. E. Gregorich, C. E. Düllmann, M. A. Garcia, J. M. Gates, S. L. Nelson, L. Stavsetra, R. Sudowe, and H. Nitsche, *Phys. Rev. C* **78**, 024605 (2008).
- [5] C. Simenel *et al.*, *Phys. Lett. B* **710**, 607 (2012).
- [6] K. Satou, H. Ikezoe, S. Mitsuoka, K. Nishio, and S. C. Jeong, *Phys. Rev. C* **65**, 054602 (2002).
- [7] W. J. Swiatecki, K. Siwek-Wilczynska, and J. Wilczynski, *Phys. Rev. C* **71**, 014602 (2005).
- [8] M. G. Itkis *et al.*, *EPJ Web Conf.* **17**, 12002 (2011), and references therein.
- [9] P. K. Sahu *et al.*, *Phys. Rev. C* **72**, 034604 (2005).
- [10] R. G. Thomas *et al.*, *Phys. Rev. C* **75**, 024604 (2007).
- [11] R. Bock *et al.*, *Nucl. Phys. A* **388**, 334 (1982).
- [12] H. G. Clerc *et al.*, *Nucl. Phys. A* **419**, 571 (1984).
- [13] R. S. Naik, W. Loveland, P. H. Sprunger, A. M. Vinodkumar, D. Peterson, C. L. Jiang, S. Zhu, X. Tang, E. F. Moore, and P. Chowdhury, *Phys. Rev. C* **76**, 054604 (2007).
- [14] E. M. Kozulin *et al.*, *Instrum. Exp. Tech.* **51**, 44 (2008).
- [15] N. Colonna *et al.*, *Nucl. Instrum. Methods Phys. Res., Sect. A* **381**, 472 (1996).
- [16] See, e.g., M. L. Roush *et al.*, *Nucl. Instrum. Methods* **31**, 112 (1964), and references therein.
- [17] G. Pasquali *et al.* (unpublished).
- [18] D. J. Hinde, M. Dasgupta, J. R. Leigh, J. C. Mein, C. R. Morton, J. O. Newton, and H. Timmers, *Phys. Rev. C* **53**, 1290 (1996).
- [19] E. Mordhorst, M. Strecker, H. Froeben, M. Gasthuber, W. Scobel, B. Gebauer, D. Hilscher, M. Lehmann, H. Rossner, and T. Wilpert, *Phys. Rev. C* **43**, 716 (1991).
- [20] V. E. Viola, K. Kwiatkowski, and M. Walker, *Phys. Rev. C* **31**, 1550 (1985).
- [21] A. Al-Adili, F.-J. Hamsch, S. Pomp, and S. Oberstedt, *Phys. Rev. C* **86**, 054601 (2012).
- [22] G. N. Knyazheva, E. M. Kozulin, R. N. Sagaidak, A. Yu. Chizhov, M. G. Itkis, N. A. Kondratiev, V. M. Voskressensky, A. M. Stefanini, B. R. Behera, L. Corradi, E. Fioretto, A. Gadea, A. Latina, S. Szilner, M. Trotta, S. Beghini, G. Montagnoli, F. Scarlassara, F. Haas, N. Rowley, P. R. S. Gomes, and A. Szanto de Toledo, *Phys. Rev. C* **75**, 064602 (2007).
- [23] M. G. Itkis and A. Ya. Rusanov, *Phys. Part. Nucl.* **29**, 160 (1998).
- [24] D. Hilscher, J. R. Birkelund, A. D. Hoover, W. U. Schröder, W. Wilcke, J. R. Huizenga, A. C. Mignerey, K. L. Wolf, H. F. Breuer, and V. E. Viola, Jr., *Phys. Rev. C* **20**, 576 (1979).
- [25] D. Hilscher and H. Rossner, *Ann. Phys. Fr.* **17**, 471 (1992).
- [26] A. Saxena *et al.*, *Nucl. Phys. A* **730**, 299 (2004).
- [27] D. J. Hinde, D. Hilscher, H. Rossner, B. Gebauer, M. Lehmann, and M. Wilpert, *Phys. Rev. C* **45**, 1229 (1992).
- [28] L. Donadille *et al.*, *Nucl. Phys. A* **656**, 259 (1999).
- [29] D. J. Hinde, H. Ogata, M. Tanaka, T. Shimoda, N. Takahashi, A. Shinohara, S. Wakamatsu, K. Katori, and H. Okamura, *Phys. Rev. C* **39**, 2268 (1989).
- [30] D. J. Hinde, R. du Rietz, and M. Dasgupta, *EPJ Web Conf.* **17**, 04001 (2011).
- [31] H. Rossner, D. Hilscher, and D. J. Hinde, *Phys. Rev. C* **43**, 2434 (1991).
- [32] A. Gavron, *Phys. Rev. C* **21**, 230 (1980).
- [33] H. Feldmeier, *Rep. Prog. Phys.* **50**, 915 (1987).